Communication

The Influence of Ti^{4+} Doping on the Electrical Conductivity and Synthetic Kinetics of $NiFe_2O_4$ Powders

LI LI, XUAN LIU, RONGMEI LI, and SHULAN WANG

$NiFe_2O_4$ was synthesized from NiO and Fe_2O_3 powders by solid-state reaction. Different doping concentrations of Ti^{4+} were achieved with the addition of 0.5 to 1 wt pct TiO_2. Their electrical conductivities in the synthetic process were monitored to calculate the rate coefficient and activation energy of the synthetic reaction of $NiFe_2O_4$. The influence of Ti^{4+} doping on electrical conductivity and synthetic kinetics of $NiFe_2O_4$ was investigated. Some ideas about the design of defect structure were also introduced in brief.

DOI: 10.1007/s40553-014-0005-x

Currently, the development of electrometallurgical aluminum production requires the application of anode materials that have high chemical and thermal stability, high electrical conductivity, and low economical cost.[1–4] Meanwhile, the anode materials with little greenhouse gas emission during the electrolysis process are desirable for relief of the atmosphere pollution and climate change.[1] Nickel ferrite ($NiFe_2O_4$) is a potential candidate of the green anode material because of its high electrochemical stability and high corrosion resistance in molten cryolite-alumina.[5,6] As a spinel ferrite of the MFe_2O_4 type, $NiFe_2O_4$ is well-known for its magnetic applications in data storage, magnetic resonance imaging (MRI) enhancement, drug delivery, *etc.*[7–11] Applications of $NiFe_2O_4$ as an energy material also attract increasing attention. The substitution of metals into spinel ferrite is beneficial for improvement of the separation of photo-generated charge carriers in inactive $NiFe_2O_4$, expanding its potential application for solar energy conversion.[12] Meanwhile, its narrow band gap (2.19 eV) and outstanding magnetic properties enable it to couple with semiconductors for design of separable photocatalysts.[13,14] $NiFe_2O_4$ also has other energy-related applications, *e.g.*, decomposition of CO_2 and as anode materials for lithium ion batteries.[15–17] The synthesis of micro/nano scaled $NiFe_2O_4$ powders was achieved with different methods, such as the citrate gel process,[18] co-precipitation,[19] sol–gel,[8,20] hydrothermal,[21–23] sonomechanical,[24] and RF thermal plasma touch.[25] In addition, $NiFe_2O_4$ in different morphologies, such as nanofiber,[26,27] thin film,[28,29] nanowire,[30] and nanocube[31] was also studied. Compared with the methods discussed above, solid-state reaction is considered as a simple and economically feasible method for processing of $NiFe_2O_4$ powders.[5,32] Different additives, such as CaO[33] and MnO_2[34] were mixed with $NiFe_2O_4$ for improvement of properties. Influence of Ti substitution on the magnetic properties of $NiFe_2O_4$ is also reported.[35,36] In the current work, $NiFe_2O_4$ was doped with Ti^{4+} by solid-state reaction. The corresponding electrical conductivity of the powders with different addition amounts of TiO_2 was measured. The synthetic reaction kinetics of doped and undoped $NiFe_2O_4$ was investigated by studying the influence of Ti^{4+} doping on the properties of $NiFe_2O_4$ powders. We believe the investigation of Ti^{4+} doping on $NiFe_2O_4$ reveals the influence of defect structures on MFe_2O_4 spinel ferrite, and thus provides some guidance for the selection of dopants for the optimization of the physicochemical properties of $NiFe_2O_4$. This study will extend its applications as an energy material in fields of energy conversion and storage, including as the efficient photocatalyst or as the anode material for lithium ion batteries, *etc.*

Commercially available iron oxide (Fe_2O_3, >99.0 pct, Sigma Aldrich) and nickel oxide (NiO, >99.0 pct, Alfa Aesar) were mixed with appropriate molar ratio (1: 1), and ball milled in ethanol for 24 h. Different amounts of titanium oxide (TiO_2, >99.0 pct, Sigma Aldrich) with fixed weight percentage were added into the mixture for Ti^{4+} doping. The dried mixture was then compressed uniaxially into pellets (15 mm in diameter and 4 mm in thickness) at 158 MPa and calcined at 1213 K (940 °C) for 6 h. Fe_2O_3 and NiO powders were also pelleted and calcined at the same temperature. To analyze the reaction kinetics of $NiFe_2O_3$, the electrical conductivity of $NiFe_2O_4$ synthesized at different temperatures with variation in time was recorded by multimeter (Agilent 34401A). Two platinum plates (1 cm^2 in area) were loaded onto the two sides of the pellets as the electrode and platinum wires were used as electrode leads. The schematic of measurement was shown in Figure 1(a). X-ray diffraction (XRD), with a Philips PW3040/60 diffractometer and Cu K_α irradiation (λ = 0.15406 nm), was conducted to analyze the phase composition and microstructure of annealed $NiFe_2O_4$ powders with and without the addition of TiO_2. The analysis was operated at 40 kV and 40 mA, with a scanning rate of 0.03 min^{-1} and 2θ ranging from 20 to 70 deg. The surface morphology of the samples was detected by scanning electron microscope (SEM, Shimadzu, SSX550) at the accelerating voltage of 30 kV. The SEM was equipped with an energy dispersive X-ray spectroscopy (EDX) (INCA, Oxford Instruments) for element analysis that was used to determine the composition of the materials.

The XRD patterns of undoped and Ti-doped $NiFe_2O_4$ (0.5 wt pct addition) synthesized at 1213 K (940 °C) were shown in Figure 1(b). All diffraction

LI LI, Postdoctoral Associate, is with the Department of Materials Science and Engineering, Cornell University, Ithaca, NY 14850. XUAN LIU, Ph.D. Student, is with the Department of Materials Science and Engineering, Carnegie Mellon University, Pittsburgh, PA 15213. RONGMEI LI, Master Student, and SHULAN WANG, Professor, are with the Department of Chemistry, School of Science, Northeastern University, Shenyang 110819, China. Contact e-mail: slwang@mail.neu.edu.cn

Manuscript submitted October 11, 2013.
Article published online February 11, 2014

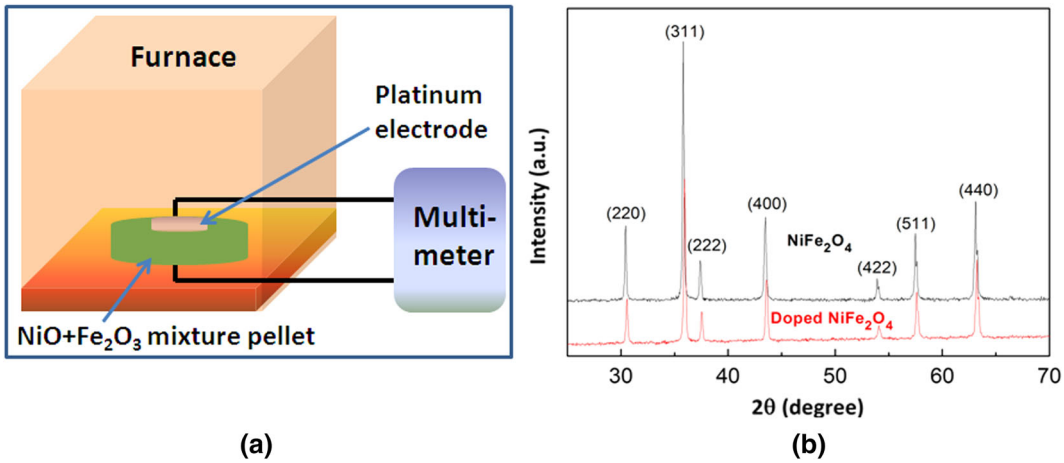

Fig. 1—(*a*) Schematic of conductivity measurement for $NiFe_2O_4$ and its control; (*b*) X-ray diffraction patterns of undoped and doped $NiFe_2O_4$ (0.5 wt pct TiO_2 addition) synthesized at 1213 K (940 °C).

peaks can be indexed to the standard pattern of $NiFe_2O_4$ (JCPDS01-086-2267). No extra peaks were observed in the diffraction pattern. This indicates that Ti has been completely dissolved into $NiFe_2O_4$. However, it also can be observed from the diffraction pattern that the peaks of Ti-doped $NiFe_2O_4$ has a small shift to the high angle, indicating that the introduction of Ti^{4+} into $NiFe_2O_4$ crystal structure leads to the decrease of the lattice constant and shrinkage of cell volume. Considering that the ionic radius of Ti^{4+} (0.68 Å) is smaller than that of Ni^{2+} (0.78 Å) and is comparable to that of Fe^{3+} (0.64 Å),[37,38] it is reasonable to believe that Ti^{4+} has been successfully doped into the $NiFe_2O_4$ structure. The most intense 2θ peak located at 35.8 deg was indexed to the (311) plane of $NiFe_2O_4$. It was used to calculate the grain size of the samples with Scherrer equation.[39] The grain sizes of undoped and doped $NiFe_2O_4$ are 57.70 and 51.22 nm, respectively, showing the influence of Ti^{4+} doping on the grain growth of $NiFe_2O_4$. The particle size and surface morphology of undoped and doped $NiFe_2O_4$ (0.5 wt pct TiO_2 addition) was investigated using SEM and the results were shown in Figures 2(a) and (b), respectively. The aggregated particle size of synthesized $NiFe_2O_4$ is in the range of 200 to 500 nm. Compared with undoped $NiFe_2O_4$, the particle size of the Ti-doped sample is slightly smaller. Notice that the size obtained from SEM is the aggregated particle size and this value is different from the nanocrystalline size provided by XRD.[40] The corresponding element analysis of doped $NiFe_2O_4$ with 0.5 and 1 wt pct TiO_2 addition was conducted with EDX and the results were shown in Figures 2(c) and (d). In addition to the peaks related to Ni, Fe, and O, the signal from Ti can also be clearly observed in both samples, indicating the presence of Ti in the doped $NiFe_2O_4$. No peak corresponding to impurities is detected. Meanwhile, the intensities of Ti peaks are also enhanced with the increase in doping concentrations. The weight percentage of Ti in (c) and (d) is 0.29 ± 0.02 and 0.62 ± 0.03 wt pct, respectively, which are consistent with the doping contents.

The electrical conductivity of undoped and doped $NiFe_2O_4$ (0.5 and 1 wt pct TiO_2 additions) as well as Fe_2O_3 and NiO at 1213 K (940 °C) were shown in Figure 3(a). All $NiFe_2O_4$ samples are initially the mixture of Fe_2O_3 and NiO (with different amounts of TiO_2 for doped samples), which were gradually converted into $NiFe_2O_4$ under solid-state reaction at 1213 K (940 °C). It can be observed that the electrical conductivity of all $NiFe_2O_4$ samples is higher than that of their components, which is a constant value during calcination. The electrical conductivity for all $NiFe_2O_4$ samples showed drastic increase in the initial 100 minutes and then the increasing trend slowed down with time. Compared with the undoped $NiFe_2O_4$, the samples with different doping concentrations show higher electrical conductivity. The best electrical property was achieved with a doping content of 0.5 wt pct TiO_2. The electrical conductivities for all samples remain constant after 6 hours and did not show further increase with reaction time.

Some of the diffusion-controlled solid reactions follow the first order.[41–43] The reaction rate in steady diffusion can be expressed using the following equation:

$$dC/dt = k(C_0 - C), \qquad [1]$$

where C_0 is the initial concentration of reactants, C the concentration of reactants at time t, and k the reaction rate coefficient. The first-order integration of above equation is shown in Eq. [2].

$$-\ln(C_0 - C) + \text{Constant} = kt. \qquad [2]$$

Based on results shown in Figure 3(a), it can be observed that $NiFe_2O_4$ shows higher electrical conductivity than NiO and Fe_2O_3. Assuming all NiO and Fe_2O_3 can be converted into $NiFe_2O_4$ and no conductive phase is further produced, the electrical conductivity changes with the synthesis of $NiFe_2O_4$ and thus reaches the maximum value when all reactants are converted into the ferrite powders. In other words, the change in

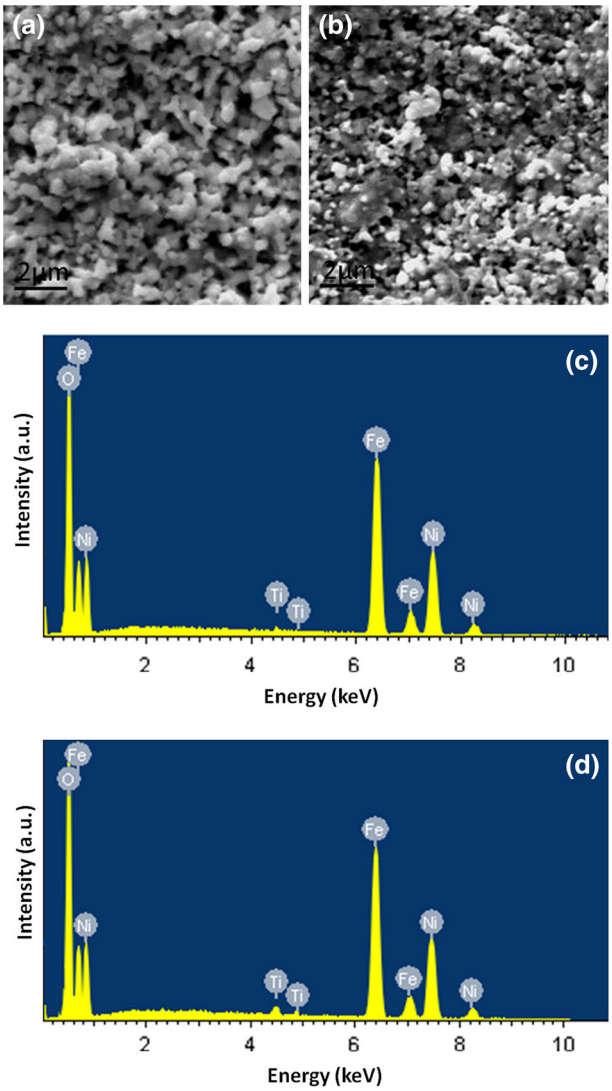

Fig. 2—SEM images of (*a*) undoped, (*b*) doped $NiFe_2O_4$ (0.5 wt pct TiO_2 addition) synthesized at 1213 K (940 °C) and EDX spectra of doped $NiFe_2O_4$ with (*c*) 0.5 wt pct as well as (*d*) 1 wt pct TiO_2 addition.

electrical conductivity with reaction time was used to characterize the synthetic kinetics of $NiFe_2O_4$. The solid-state reaction between NiO and Fe_2O_3 for production of $NiFe_2O_4$ is shown as follows:

$$\begin{array}{llll} \mathrm{NiO} + \mathrm{Fe_2O_3} = \mathrm{NiFe_2O_4} & & & \\ t = 0 & n_0 & 0 & \kappa_0 \\ 0 & n_t = n_0 - x & x & \kappa_t \\ t = \infty & 0 & n_0 & \kappa_\infty \end{array} .$$

Herein, n_0 and x are the initial amount of Fe_2O_3 and the amount of Fe_2O_3 consumed at time t, while κ_0, κ_t, and κ_∞ represent the electrical conductivities of the samples in the initial stage, at time t and at the time when the solid-state reaction is complete. The variation in electrical conductivity can be correlated to the concentration of reactants, as shown in Eqs. [3] and [4]:

$$\kappa_\infty - \kappa_0 \propto n_0 \propto C_0, \quad [3]$$

$$\kappa_t - \kappa_0 \propto n_t \propto C. \quad [4]$$

Therefore, the change of electrical conductivity reflects the synthetic process of the diffusion-controlled solid-state reaction through the following relationship:

$$-\ln(\kappa_\infty - \kappa_t) + \text{Constant} = kt. \quad [5]$$

The logarithm of the electrical conductivity variation for undoped and doped $NiFe_2O_4$ synthesized at 1213 K (940 °C) was plotted with time in Figure 3(b). It can be observed that the variation of electrical conductivity of synthesized $NiFe_2O_4$ is linearly proportional to the measurement time, which is consistent with the model discussed above. The initial 30 minutes were used to achieve the thermal equilibrium between reactants. The electrical conductivity of the reactants at 8 hours was noted as κ_∞. The reaction coefficient of $NiFe_2O_4$ doped with Ti^{4+} is larger than the undoped sample, indicating the promotion of the solid-state reaction with the addition of Ti^{4+}.

The kinetics of the diffusion-controlled solid-state reaction for the synthesis of $NiFe_2O_4$ follows the Arrhenius equation, as shown in Eq. [6]:

$$\ln k = -E/RT + A, \quad [6]$$

where k is the reaction rate coefficient, E the activation energy, T the absolute temperature, R the universal gas constant, and A a model constant. The logarithm relationship between the reaction rate coefficient and the inverse of reaction temperature ($1/T$) was studied systematically and shown in Figure 4. It can be clearly observed that the logarithm rate coefficient is linearly correlated with the inverse of reaction temperature for all samples and that Ti^{4+} doping leads to the increase in reaction rate for the synthesis of $NiFe_2O_4$. However, the highest reaction rate was achieved for the sample doped with 0.5 wt pct TiO_2, while higher doping concentration leads to decrease in reaction rate. The average activation energy, calculated from the slope of curves in Figure 3, was 53.1, 45.5, and 47.0 kJ mol^{-1} for 0, 0.5, and 1 wt pct TiO_2 addition. The reaction rate coefficients for the synthetic reaction of $NiFe_2O_4$ at different temperatures and with different additions of TiO_2 are listed in Table I. All reaction rate coefficients increased with the increase of temperature because the diffusion-controlled solid-state reaction is thermally activated.

It is interesting to note that the electrical conductivity of $NiFe_2O_4$ is influenced by its doping concentration while the electrical conductivity variation is used to track the kinetics of solid-state synthesis for ferrite powders. The electrical conductivity increased dramatically in the initial period, indicating that the reaction rate between NiO and Fe_2O_3 is high in the first 100 minutes. However, with production of more and more $NiFe_2O_4$ powders, the diffusion between NiO and Fe_2O_3 is hindered, and their diffusion distance is thus

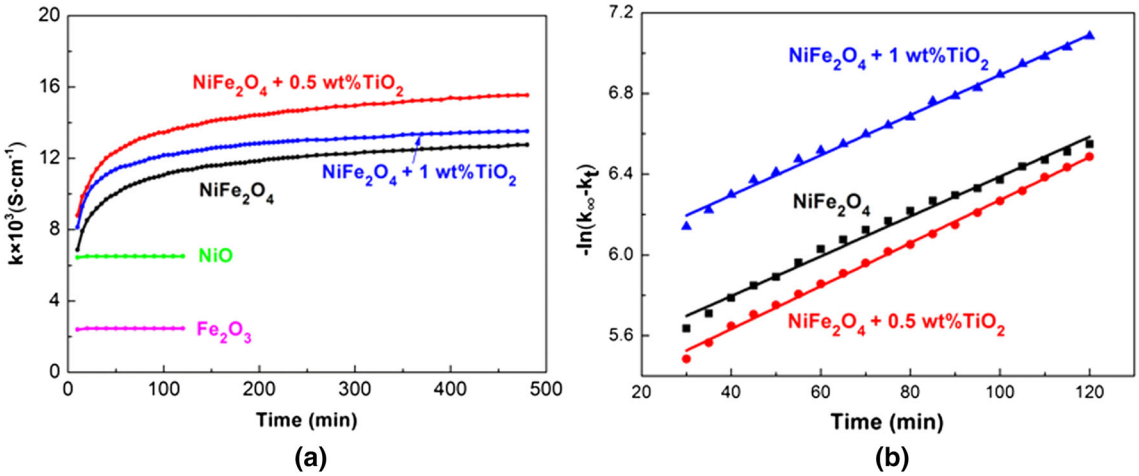

Fig. 3—(*a*)Electrical conductivity of undoped/doped $NiFe_2O_4$ and their components at 1213 K (940 °C). (*b*) Logarithm of the variation in electrical conductivity for undoped and doped $NiFe_2O_4$ samples synthesized at 1213 K (940 °C).

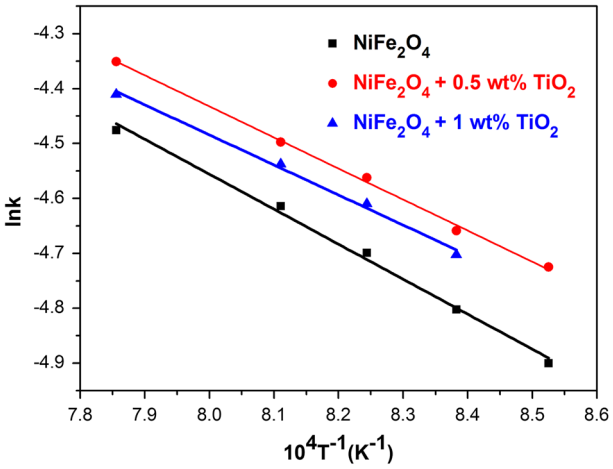

Fig. 4—Logarithm relationships of the rate coefficient with the inverse of reaction temperature for synthesis of undoped and doped $NiFe_2O_4$.

Table I. Reaction Rate Coefficient (*k*) of the $NiFe_2O_4$ Synthetic Reaction at Different Temperatures

Temperature [K (°C)]	*k* Value for $NiFe_2O_4$ with Different Doping Concentrations (min^{-1})		
	0 wt pct TiO_2	0.5 wt pct TiO_2	1 wt pct TiO_2
1173 (900)	0.007446	0.008871	—
1193 (920)	0.008215	0.009474	0.009071
1213 (940)	0.009102	0.01044	0.009950
1233 (959)	0.009911	0.01114	0.01071
1273 (1000)	0.01138	0.01290	0.01214

increased for the reaction. Therefore, the increase in reaction rate is slowed down. The electrical conductivity does not show any further change when the solid-state reaction is complete.

In the inverse spinel structure of $NiFe_2O_4$, half of the Fe^{3+} cations occupy the tetrahedral A site while the rest Fe^{3+} and Ni^{2+} cations in a short range order are considered to distribute on the octahedral B site.[44] The addition of TiO_2 into $NiFe_2O_4$ is prone to form cation defect rather than oxygen vacancy because the oxygen diffusion rate is small compared with that of cations.[45] Introduction of Ti^{4+} into the crystal structure of $NiFe_2O_4$ can substitute both Fe^{3+} and Ni^{3+} sites,[36] and the electrical conductivity is increased by providing more conducting electrons and enhancing the hopping rate of electrons between different sites. Another reason for the increase of electrical conductivity with the inclusion of Ti^{4+} may be attributed to the increase in charge interexchange in $NiFe_2O_4$ powders. The conducting mechanism of nickel ferrite can be explained by the redox reaction between Fe^{3+}/Fe^{2+} and Ni^{3+}/Ni^{2+}.[1] The introduction of Ti^{4+} has the intervalance charge transfer between Ti^{4+}/Ti^{3+} and Fe^{3+}/Fe^{2+},[35] promoting the charge exchange between different sites and enhancing the conductivity of doped samples. From this point of view, the activation energy of the synthetics reaction should be positively proportional to the hopping energy of electron. The reaction with the smallest activation energy should have the lowest hopping energy of electron. The third reason for the increase in electrical conductivity with Ti^{4+} doping may be attributed to the shrinkage of lattice constant and cell volume for $NiFe_2O_4$ powders. Assuming the ions do not vibrate from their original positions greatly, this shrinkage decreases the average separation distances between different ions, leading to the decrease of average electron hopping distance and increase in the electrical conductivity.[46]

The influence of Ti^{4+} doping on the physical properties of $NiFe_2O_4$ is strongly dependent on the doping concentration. High doping concentration may lead to the formation of secondary phase on the surface of Fe^{3+} grains, influence the charge interexchange of the ferrite powders and decrease the hopping rate of electrons.[46,47]

Therefore, the electrical conductivity of $NiFe_2O_4$ drops with high doping concentrations. In addition, the meager amounts of ferrous and ferric ions at the B site may be another reason leading to the decrease of conductivity with increase in the doping concentration.[1]

The introduction of dopant has many influences on the properties of ferrite materials. The process for the change of physiochemical properties is complex and is a result of different synergic factors in most cases. Therefore, the exact influence of dopants is difficult to estimate. Herein, we want to provide some general ideas for the selection of dopants to adjust the electrical conductivity of ferrite powders. The first factor of consideration is the ionic radius. The ionic radius influences the lattice parameters and porosity of the ferrite samples. It is reported that ions with larger radius is prone to form the secondary phase on the surface of ferrite grains, although the formation of the secondary phase is strongly dependent on the dopant concentration, sintering processing as well as other factors.[47] Meanwhile, the increase in porosity of the samples hinders the electron transfer through the crystal and thus is not beneficial for the improvement of electrical conductivity. However, the exact influence of ionic radius on the electrical conductivity is still not clear. Another factor for consideration of dopant selection is the charge. The cation defect is commonly formed in ferrite powders and the charge of dopant influences the hopping of electrons between ions. The high charge Bi^{5+} substitution is reported to decrease the electrical conductivity of nickel-zinc ferrites.[46] Both Mg^{2+} and Ce^{3+} dopants are observed to increase the electrical conductivity of $NiFe_2O_4$ with appropriate doping concentrations.[48] The rare earth elements of R^{3+} are also widely studied as possible dopants and their inclusion leads to the increase in resistivity.[49,50] Other factors, such as the electronic structure of dopants,[48] and the solubility in the compound, should also be carefully considered to control the physicochemical properties of ferrite compounds. Currently, different dopants are used to improve the properties of ferrite powders, such as electrical,[48] magnetic,[49] photoelectrical,[51] sensing,[52] and catalytic properties.[1] The study shown here provides new ideas and strategies for selection of dopants to extend the application of ferrite in energy conversion and storage.

To conclude, $NiFe_2O_4$ powders were synthesized from NiO and Fe_2O_3 *via* solid-state reaction at 1213 K (940 °C). Ti^{4+} was doped into the atomic structure of $NiFe_2O_4$ with the addition of 0.5 to 1.0 wt pct TiO_2. The doped $NiFe_2O_4$ showed high electrical conductivity and the influence of different doping amounts was analyzed. The diffusion-controlled solid-state reaction for synthesis of $NiFe_2O_4$ follows the first-order kinetics. The activation energy of the synthetic reaction is 45.5 to 53.1 kJ mol^{-1} and the rate coefficient is 0.007 to 0.012 min^{-1}. Ti^{4+} doping decreased the activation energy and increased the rate coefficient. The influential factors for design of the defect structure are discussed in brief. This study provides new ideas for optimizing the physicochemical properties of ferrite compounds and extending their applications as energy materials for energy storage and conversion.

This work was supported by National Natural Science Foundation of China No. 51274058.

REFERENCES

1. L.J. Berchmans, R.K. Selvan, and C.O. Augustin: *Mater. Lett.*, 2004, vol. 58, pp. 1928–33.
2. E. Olsen and J. Thonstad: *J. Appl. Electrochem.*, 1999, vol. 29, pp. 293–99.
3. D.R. Sadoway: *JOM*, 2001, vol. 53, pp. 34–35.
4. H. Xiao, R. Hovland, S. Rolseth, and J. Thonstad: *Metall. Mater. Trans. B*, 1996, vol. 27B, pp. 185–93.
5. Z. Zhang, Y. Liu, G. Yao, G. Zu, and Y. Hao: *Int. J. Appl. Ceram. Technol.*, 2013, vol. 10, pp. 142–49.
6. W. Li, G. Zhang, J. Li, and Y. Lai: *JOM*, 2009, vol. 61, pp. 39–43.
7. K.A. Pettigrew, J.W. Long, E.E. Carpenter, C.C. Baker, J.C. Lytle, C.N. Chervin, M.S. Logan, R.M. Stroud, and D.R. Rolison: *ACS Nano*, 2008, vol. 2, pp. 784–90.
8. S. Maensiri, C. Masingboon, B. Boonchom, and S. Seraphin: *Scripta Mater.*, 2007, vol. 56, pp. 797–800.
9. V. Sepelak, I. Bergmann, A. Feldhoff, P. Heitjans, F. Krumeich, D. Menzel, F.J. Litterst, S.J. Campbell, and K.D. Becker: *J. Phys. Chem. C*, 2007, vol. 111, pp. 5026–33.
10. E. Terreno, D.D. Castelli, A. Viale, and S. Aime: *Chem. Rev.*, 2010, vol. 110, pp. 3019–42.
11. Q. Liu, H. Huang, L. Lai, J. Sun, T. Shang, Q. Zhou, and Z. Xu: *J. Mater. Sci.*, 2009, vol. 44, pp. 1187–91.
12. K.N. Harish, H.S. Bhojya Naik, P.N. Prashanth Kumar, and R. Viswanath: *ACS Sustain. Chem. Eng.*, 2013, vol. 1, pp. 1143–53.
13. Y. Fu, H. Chen, X. Sun, and X. Wang: *AlChE J.*, 2012, vol. 58, pp. 3298–305.
14. Y.S. Chung, S.B. Park, and D.-W. Kang: *Mater. Chem. Phys.*, 2004, vol. 86, pp. 375–81.
15. H.C. Shin, J.H. Oh, B.C. Choi, and S.C. Choi: *Phys. Status Solidi C*, 2004, vol. 1, pp. 3748–53.
16. C. Vidal-Abarca, P. Lavela, and J.L. Tirado: *J. Phys. Chem. C*, 2010, vol. 114, pp. 12828–32.
17. H. Zhao, Z. Zheng, K.W. Wong, S. Wang, B. Huang, and D. Li: *Electrochem. Commun.*, 2007, vol. 9, pp. 2606–10.
18. S. Prasad and N.S. Gajbhiye: *J. Alloys Compd.*, 1998, vol. 265, pp. 87–92.
19. K. Maaz, S. Karim, A. Mumtaz, S.K. Hasanain, J. Liu, and J.L. Duan: *J. Magn. Magn. Mater.*, 2009, vol. 321, pp. 1838–42.
20. D.-H. Chen and X.-R. He: *Mater. Res. Bull.*, 2001, vol. 36, pp. 1369–77.
21. J. Huo and M. Wei: *Mater. Lett.*, 2009, vol. 63, pp. 1183–84.
22. S. Komarneni, E. Fregeau, E. Breval, and R. Roy: *J. Am. Ceram. Soc.*, 1988, vol. 71, pp. C26–C28.
23. J. Zhou, J. Ma, C. Sun, L. Xie, Z. Zhao, H. Tian, Y. Wang, J. Tao, and X. Zhu: *J. Am. Ceram. Soc.*, 2005, vol. 88, pp. 3535–37.
24. K.V.P.M. Shafi, Y. Koltypin, A. Gedanken, R. Prozorov, J. Balogh, J. Lendvai, and I. Felner: *J. Phys. Chem. B*, 1997, vol. 101, pp. 6409–14.
25. S. Son, M. Taheri, E. Carpenter, V.G. Harris, and M.E. McHenry: *J. Appl. Phys.*, 2002, vol. 91, pp. 7589–91.
26. C.-Y. Zhang, X.-Q. Shen, J.-X. Zhou, M.-X. Jing, and K. Cao: *J. Sol Gel. Sci. Technol.*, 2007, vol. 42, pp. 95–100.
27. D. Li, T. Herricks, and Y. Xia: *Appl. Phys. Lett.*, 2003, vol. 83, pp. 4586–88.
28. S. Venzke, R.B. van Dover, J.M. Phillips, E.M. Gyorgy, T. Siegrist, C.H. Chen, D. Werder, R.M. Fleming, R.J. Felder, and E. Coleman: *J. Mater. Res.*, 1996, vol. 11, pp. 1187–98.
29. U. Luders, A. Barthelemy, M. Bibes, K. Bouzehouane, S. Fusil, E. Jacquet, J.-P. Contour, J.-F. Bobo, J. Fontcuberta, and A. Fert: *Adv. Mater.*, 2006, vol. 18, pp. 1733–36.

30. P. Sivakumar, R. Ramesh, A. Ramanand, S. Ponnusamy, and C. Muthamizhchelvan: *Mater. Lett*., 2012, vol. 66, pp. 314–17.
31. C. Xiangfeng, J. Dongli, and Z. Chenmou: *Sens. Actuator B*, 2007, vol. 123, pp. 793–97.
32. A. Ceylan, S. Ozcan, C. Ni, and S. Ismat Shah: *J. Magn. Magn. Mater*., 2008, vol. 320, pp. 857–63.
33. J. Li, G. Zhang, Y. Lai, Y. Zhang, and Z. Tian: *J. Cent. South Univ*., 2007, vol. 14, pp. 629–32.
34. E. Rezlescu, N. Iftimie, P.D. Popa, and N. Rezlescu: *J. Phys. Conf. Ser*., 2005, vol. 15, pp. 51–54.
35. M. Seki, A.K.M. Hossain, T. Kawai, and H. Tabata: *J. Appl. Phys*., 2005, vol. 97, p. 083541.
36. P. Chand, R.C. Srivastava, and A. Upadhyay: *J. Alloys Compd*., 2008, vol. 460, pp. 108–14.
37. M.T. Buscaglia, V. Buscaglia, M. Viviani, P. Nanni, and M. Hanuskova: *J. Eur. Ceram. Soc*., 2000, vol. 20, pp. 1997–2007.
38. J. Li, Z. Tang, and Z. Zhang: *Electrochem. Commun*., 2005, vol. 7, pp. 894–99.
39. A.L. Patterson: *Phys. Rev*., 1939, vol. 56, p. 978.
40. K.V. Baiju, S. Shukla, K.S. Sandhya, J. James, and K.G.K. Warrier: *J. Phys. Chem. C*, 2007, vol. 111, pp. 7612–22.
41. J.H. Sharp, G.W. Brindley, and B.N.N. Achar: *J. Am. Ceram. Soc*., 1966, vol. 49, pp. 379–82.
42. J. Sestak and G. Berggren: *Thermochim. Acta*, 1971, vol. 3, pp. 1–12.
43. A. Khawam and D.R. Flanagan: *J. Phys. Chem. B*, 2006, vol. 110, pp. 17315–28.
44. V.G. Ivanov, M.V. Abrashev, M.N. Iliev, M.M. Gospodinov, J. Meen, and M.I. Aroyo: *Phys. Rev. B*, 2010, vol. 82, p. 024104.
45. S.R. Summerfelt and C.B. Carter: *J. Am. Ceram. Soc*., 1992, vol. 75, pp. 2244–50.
46. M. Pal, P. Brahma, and D. Chakravorty: *J. Magn. Magn. Mater*., 1996, vol. 152, pp. 370–74.
47. M.A. Ahmed, E. Ateia, and S.I. El-Dek: *Mater. Lett*., 2003, vol. 57, pp. 4256–66.
48. G. Dixit, J.P. Singh, C.L. Chen, C.L. Dong, R.C. Srivastava, H.M. Agrawal, W.F. Pong, and K. Asokan: *J. Alloys Compd*., 2013, vol. 581, pp. 178–85.
49. K.K. Bharathi, G. Markandeyulu, and C.V. Ramana: *J. Phys. Chem. C*, 2011, vol. 115, pp. 554–60.
50. O.M. Hemeda, M.Z. Said, and M.M. Barakat: *J. Magn. Magn. Mater*., 2001, vol. 224, pp. 132–42.
51. C.H. Kim, Y. Myung, Y.J. Cho, H.S. Kim, S.-H. Park, J. Park, J.-Y. Kim, and B. Kim: *J. Phys. Chem. C*, 2009, vol. 113, pp. 7085–90.
52. Y.-L. Liu, H. Wang, Y. Yang, Z.-M. Liu, H.-F. Yang, G.-L. Shen, and R.-Q. Yu: *Sens. Actuator B*, 2004, vol. 102, pp. 148–54.